Insertion of the Methylene-oxy Surrogate of the Amide Bond into Boc-Val-Leu-OH: X-Ray Crystal Structure, Solution Conformation and Molecular Modelling Study

Gérald Villeneuve,†[a] John DiMaio,[b] Marc Drouin[c] and André G. Michel[c]
[a] *Department of Chemistry, McGill University, Montréal, Québec, H3A 2K6, Canada*
[b] *Institut de Recherche en Biotechnologie, Montréal, Québec, H4P 2R2, Canada*
[c] *Département de Chimie, Université de Sherbrooke, Sherbrooke, Québec, J1K 2R1, Canada*

The conformational features associated with the introduction of the methylene-oxy surrogate of the amide bond were explored by studying the crystal and solution conformation of the related model peptides Boc-Val-Leu-OH (**1**) and Boc-Val-$\psi(CH_2O)$-Leu-OH (**2**). Two independent molecular conformations were found for **1** in the crystal state whereas one was found for its congener **2**. In compound **2** the dihedral angle defined by C^{α}–CH_2–O–C^{α} (ω') adopts a value of −165.7(3)°, close to the situation encountered in the classical amide bond. 2D NOE NMR studies suggest that the preferred backbone conformation of **2** in [$^2H_6$]DMSO correlates with the crystal structure whereas the preferred backbone conformation of **1** in [$^2H_6$]DMSO showed a departure from its crystalline conformation. Molecular mechanics computations demonstrate the effect of the short $C(sp^3)$–$O(sp^3)$ bond in compound **2** in dictating the preferred dihedral angle values adopted by ω' and φ_{Leu}.

A major goal in the quest toward understanding the inherent function or mechanism of regulatory peptides such as receptor ligands or enzyme inhibitors relies on the elucidation of their bioactive conformation. To this end, the study of constrained analogues of agonist or antagonist molecules has been useful in deciphering the conformational requirements at the level of the acceptor macromolecule.[1] Constraints can be global such as in the bridging of two remote amino acids[2] or more confined to individual amino acid modifications.[3] Local constraints have been obtained through C^{α} inverted configuration, N and C^{α} methyl substitutions, insertion of proline or related imino acids and by the use of modified amino acid side chains.

More recently, local modifications have centred on the amide bond itself and several surrogate structures have been proposed.[4] Amide bond replacements have become attractive tools in efforts directed at conferring proteolytic resistance while others impart transition state character to the normal scissile amide bond and therefore have produced powerful protease inhibitors.[5] Amide bond surrogates which do not possess the double bond character can be expected to be more flexible compared to the original amide.[1] This might be an advantage when a fine-tuning of the binding properties is desired but the new steric and electronic properties must be considered with care. In this regard, several studies on the conformational consequences of substituting the amide bond with various 'isosteres' have been reported previously.[6] As a continuation of our work in this field we have studied the conformational consequences stemming from the replacement of an amide bond by a methylene-oxy group in a model dipeptide. We report the comparative X-ray structures of Boc-Val-Leu-OH **1** and the related $\psi(CH_2O)$ analogue **2**.‡ We have also investigated the conformation of these compounds in [$^2H_6$]DMSO by ^1H NMR spectroscopy. In addition we have performed molecular mechanics computation based on the determined X-ray crystal structures in order to assess the relative conformational mimicry.[7] The particular dipeptide sequence was chosen since it is related to the sequence Val^2-Sta^3 of the potent aspartic protease inhibitor pepstatin A. Renin and HIV-1 protease[8] are therapeutically important enzymes that are inhibited by pepstatin.

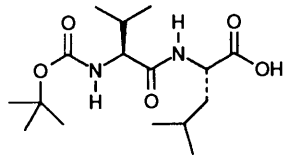

1

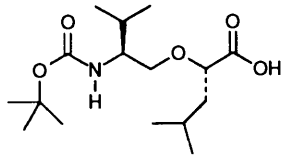

2

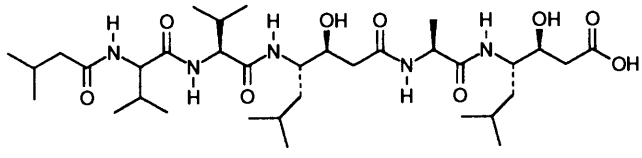

Pepstatin A

Experimental

Chemistry.—Compound **1** was prepared by the 1,3-dicyclohexylcarbodiimide (DCC) mediated coupling of Boc-Val-OH with H-Leu-OBz followed by hydrogenolysis of the benzyl ester group. Compound **2** was prepared based on the procedure reported by TenBrink[9] for similar compounds and using in our case D-leucine and L-valinol as starting materials. The steps leading to compound **2** are shown in Scheme 1; all intermediates were characterized.

Equipment.—M.p.s were recorded on a Gallenkamp capillary apparatus and are uncorrected. IR spectra were recorded on a Perkin-Elmer 1600 FTIR and were taken in KBr pellets or as neat liquid. ^1H NMR spectra were recorded either at 300 or 200 MHz on Varian XL-300 or XL-200 spectrometers, respectively.

† *Present address:* Département de Chimie, Université de Sherbrooke, Sherbrooke, Québec, J1K 2R1, Canada.

‡ Boc = *tert*-Butoxycarbonyl; Val = valine; Leu = leucine; DCC = 1,3-dicyclohexylcarbodiimide; TBDMS = *tert*-butyldimethylsilyl; DMAP = 4-dimethylaminopyridine; TEA = triethylamine; HOBT = 1-hydroxybenzotriazole; DMSO = dimethyl sulfoxide. 1 cal = 4.184 J.

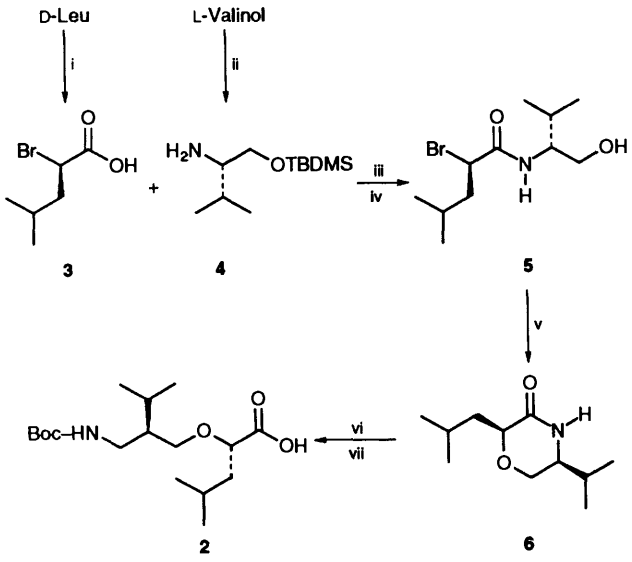

Scheme 1 *Reagents and conditions:* i, $NaNO_2$, HBr (48%), 0 °C, 30 min; ii, 0.3 equiv. DMAP, 1.1 equiv. TEA, TBDMSCl, CH_2Cl_2, 0 °C–room temp., 8 h; iii, 1.0 equiv. HOBT, 1.1 equiv. DCC, CH_2Cl_2, 0 °C–room temp., 2 h; iv, Amberlyst-15, MeOH, room temp., 2 h; v, 1.1 equiv. NaH, THF, room temp., 2 h; vi, HCl (6 mol dm^{-3}), 110 °C, 20 h; vii, 1.1 equiv. Boc_2O, dioxane–water (5%), Et_3N, room temp.

^{13}C NMR spectra were recorded at 75 MHz on a Varian XL-300 spectrometer. All NMR spectra were referenced to the residual solvent peak ($CDCl_3$ ^1H 7.24, ^{13}C 77.0; C_6D_6, ^1H 7.15, ^{13}C 128.0 ppm); *J*-values are given in Hz. ^1H NMR assignments were based on selective decoupling and 2D homoscalar correlated experiment (COSY). Spin simulation, performed with the SPINS program, was used to determine some of the coupling constants and chemical shift values. Thin layer chromatography (TLC) was carried out on glass-backed Merck silica gel 60, 0.25 mm thickness. Optical rotations were measured on a JASCO DIP-140 instrument at sodium line wavelength at 20 °C in a 0.5 dm cell and the values were integrated over a period of 60 s. $[\alpha]_D$-Values are given in units of 10^{-1} deg cm^2 g^{-1}. Mass spectra and exact masses were determined with a ZAB-1F mass spectrometer.

Reagents and Solvents.—All reagents were commercially available and were used without further purification. Tetrahydrofuran (THF) was dried by distillation from sodium–benzophenone and dichloromethane from calcium hydride.

tert-*Butoxycarbonylvalylleucine Benzyl Ester.*—L-Leucinium benzyl ester *p*-toluenesulfonate (1.97 g, 5.0 mmol), 1-hydroxybenzotriazole (0.67 g, 5.0 mmol), *tert*-butoxycarbonyl-L-valine (1.09 g, 5.0 mmol) and *N*-ethylmorpholine (0.60 cm^3, 5.0 mmol) were dissolved in dry THF (5.0 cm^3). The mixture was cooled to 0 °C and DCC (1.08 g, 5.0 mmol) was added. The reaction was allowed to proceed for 1 h at 0 °C and 1 h at room temp. The dicyclohexylurea that precipitated was filtered and the organic phase was evaporated to dryness. The yellow oil obtained was dissolved in ethyl acetate (25 cm^3) and treated sequentially with saturated $NaHCO_3$ (10 cm^3) and citric acid solution (10%; 10 cm^3). The organic phase was dried ($MgSO_4$), filtered, and evaporated under reduced pressure. Chromatography on silica gel using ethyl acetate–hexane (1:3) gave the desired product as a clear colourless thick oil which slowly solidified on standing (1.68 g, 80%). M.p. 83.5–84.5 °C (hexane); $[\alpha]_D^{20}$ −52.5 (*c* 2.0, MeOH); TLC R_f 0.37 (ethyl acetate–hexane 1:3); ν_{max}/cm^{-1} 3328 (NH), 2955 (CH), 1736 (CO), 1682 (CO), 1660 (CO), 1547, 1524, 1306, 1250 and 1173; δ_H(200 MHz; $CDCl_3$) 0.85–0.95 [12 H, m, Leu $(CH_3)_2$, Val $(CH_3)_2$], 1.411 (9 H, s, Bu^t), 1.45–1.78 (3 H, m, Leu $C^\beta H_2$, $C^\gamma H$), 2.07 (1 H, oct, *J* 6.6, Val $C^\beta H$), 3.87 (1 H, dd, *J* 8.8, 6.4, Val $C^\alpha H$), 4.65 (1 H, m, Leu $C^\alpha H$), 5.04 (1 H, d, *J* 8.9, Val NH), 5.13 (2 H, s, OCH_2Ar), 6.22 (1 H, d, *J* 8.2, Leu NH) and 7.32 (s, 5 H, Ph); δ_C($CDCl_3$) 172.45, 171.50, 155.85, 135.31, 128.54, 128.36, 128.23, 79.89, 67.03, 59.97, 50.79, 41.38, 30.77, 28.25, 24.72, 22.75, 21.80, 19.17 and 17.87; *m/z* [electron impact (EI)] 421 (MH^+), 420 (M^+), 378 ($MH^+ - C_3H_7$), 364 ($MH^+ - C_4H_9$) and 347 ($M^+ - C_4H_9O$).

tert-*Butoxycarbonylvalylleucine* (**1**).—10% Palladium over charcoal catalyst (0.17 g) was introduced into a three-neck flask previously flushed with a stream of nitrogen. *tert*-Butoxycarbonylvalylleucine benzyl ester (1.68 g, 4 mmol) was dissolved in methanol (25 cm^3) and carefully added to the catalyst. A hydrogen stream was then introduced and allowed to flow at atmospheric pressure for 4 h. The reaction mixture was filtered over Celite and the filtrate evaporated to dryness under reduced pressure. The residue was dissolved in ethyl acetate (25 cm^3) and extracted with two portions (25 cm^3) of aq. $NaHCO_3$ (5%). The free acid was recovered by addition of citric acid (Congo red) and extracted with ethyl acetate (2 × 50 cm^3). The ethyl acetate phase was treated with water (2 × 25 cm^3) and dried ($MgSO_4$) followed by evaporation under reduced pressure. Recrystallisation using diethyl ether–hexane provided pure **1** (1.04 g, 76%). M.p. 156–157 °C (diethyl ether); $[\alpha]_D^{20}$ −41.2 (*c* 2.0, MeOH); TLC R_f 0.19 (ethyl acetate–hexane 1:3 + 0.5% acetic acid); ν_{max}/cm^{-1} 3500–2400br (CO_2H) 3318 (NH), 2955 (CH), 1723 (CO), 1687 (CO), 1641 (CO), 1543, 1297, 1250 and 1166; δ_H[300 MHz; [$^2H_6$]DMSO (dimethyl sulfoxide)] see Table 4; δ_C($CDCl_3$) 175.63, 172.29, 156.25, 80.12, 60.15, 50.65, 41.13, 30.59, 28.20, 24.72, 22.79, 21.71, 19.03 and 18.24; *m/z* (EI) 331 (MH^+), 275 ($MH^+ - C_4H_8$), 257 ($M^+ - C_4H_9O$) (Found: MH^+, 331.2228. Calc. for $C_{16}H_{31}N_2O_5$: *M*, 331.2233).

(R)-2-*Bromo*-4-*methylpentanoic Acid* (**3**).—D-Leucine (2.00 g, 15.2 mmol) was dissolved in aq. HBr (48%, 16 cm^3) and water (27 cm^3). Cracked ice was added to give a total volume of 80 cm^3. The solution was stirred vigorously and $NaNO_2$ (3.1 g, 45 mmol) was added in small portion. When the reaction mixture had reached room temperature it was extracted with ether (5 × 15 cm^3). The ether phase was treated with water (2 × 20 cm^3), dried ($MgSO_4$) and the solvent was evaporated under reduced pressure. The yellowish oil (2.39 g, 80%) was distilled (b.p. 138–139 °C/20 mmHg) and gave a clear colourless oil (1.93 g, 65%); $[\alpha]_D^{20}$ +54.0 (neat); TLC R_f 0.50 (ethyl acetate–hexane 1:1); ν_{max}/cm^{-1} 3500–2400vbr (CO_2H), 1716br (CO), 1422, 1287, 1172 and 922; δ_H(200 MHz; $CDCl_3$) 0.91 (3 H, d, *J* 6.3, Me), 0.96 (3 H, d, *J* 6.4, Me), 1.79 [1 H, nonuplet, *J* 6.5, $CH_2CH(CH_3)_2$], 1.91 (2 H, t, *J* 6.6, $CHCH_2CH$), 4.28 (1 H, t, *J* 7.1, $BrCHCH_2$) and 4.5–5.5 (1 H, br exch. D_2O, CO_2H); δ_C($CDCl_3$) 175.58, 43.98, 43.15, 26.21, 22.22 and 21.44; *m/z* (EI) 181 ($M^+ + 2 - CH_3$), 179 ($M^+ - CH_3$), 140 ($M^+ + 2 - C_4H_8$), 138 ($M^+ - C_4H_8$) and 115 ($M^+ - Br$).

O-(tert-*Butyldimethylsilyl*)*valinol* (**4**).—Valinol (1.00 g, 9.7 mmol) was dissolved in dry CH_2Cl_2 (10 cm^3) and treated with triethylamine (1.18 g; 11.7 mmol) and 4-dimethylaminopyridine (0.045 g, 3.4 mmol). The mixture was cooled to 0 °C and *tert*-butyldimethylsilyl (TBDMS) chloride (1.61 g, 10.7 mmol) added. The reaction mixture was allowed to reach room temperature and was stirred for an additional 6 h. The triethylamine hydrochloride salt was filtered and the filtrate was treated with water (2 × 5 cm^3) and with aq. ammonium chloride (2 × 5 cm^3). Drying ($MgSO_4$) and evaporation under reduced pressure gave the crude product. Distillation of this

material under reduced pressure (b.p. 102–103 °C/20 mmHg) afforded the pure TBDMS alcohol (1.43 g, 68%); $[\alpha]_D^{20}$ +5.8 (neat); TLC R_f 0.40 (ethyl acetate); ν_{max}/cm^{-1} 3374w (NH), 2956, 2858s (CH), 1471, 1388, 1362, 1256, 1095s and 837; δ_H(200 MHz; $CDCl_3$) 0.05 (6 H, s, $SiMe_2$), 0.83–0.94 [6 H, d, $CH(CH_3)_2$], 0.87 (9 H, s, Bu^{t}Si), 1.5 (2 H, br s, NH_2), 1.63 [1 H, oct, *J* 6.7, $CHCH(CH_3)_2$], 2.56 (1 H, ddd, *J* 6.1, 7.7, 4.1, NCH), 3.38 (1 H, dd, *J* 7.7, ^2J −9.7, $CHCH_AH_B$) and 3.64 (1 H, dd, *J* 4.1, ^2J −9.7, $CHCH_AH_B$); $\delta_C(CDCl_3)$ 66.18, 58.29, 30.45, 25.84, 19.41, 18.27, 18.19 and −5.43; *m/z* (EI) 218 (MH^+), 217 (M^+), 202 ($M^+ - CH_3$), 174 ($M^+ - C_3H_7$) and 160 ($M^+ - C_4H_9$).

N-[(2R)-*Bromo*-4-*methylpentanoyl*]-O-(tert-*butyldimethylsilyl*)-L-*valinol*.—(*R*)-2-Bromo-4-methylpentanoic acid (**3**) (0.72 g, 3.7 mmol) and 1-hydroxybenzotriazole (0.56 g, 3.7 mmol) were dissolved in dry CH_2Cl_2 (3 cm^3) and cooled at 0 °C. DCC (0.82 g, 3.7 mmol) was added and the mixture was stirred for 2 h. *O*-(*tert*-Butyldimethylsilyl)-L-valinol (**4**) (0.80 g, 3.7 mmol) was then added and the mixture maintained at 0 °C for another 2 h. The dicyclohexylurea was filtered and the filtrate was washed with sodium hydrogen carbonate (1 mol dm^{-3}, 5 cm^3), citric acid (2 mol dm^{-3}, 5 cm^3) and water (5 cm^3). The organic phase was dried ($MgSO_4$) and evaporated to dryness under reduced pressure. The residue was dissolved in hexane and another crop of dicyclohexylurea was removed. Chromatography on silica gel (ethyl acetate–hexane 10%) yielded the pure compound as a thick oil which solidified on standing (0.65 g, 45%). M.p. 58–60 °C; $[\alpha]_D^{20}$ −11.9 (*c* 12, CH_2Cl_2); TLC R_f 0.35 (ethyl acetate–hexane 10%); ν_{max}/cm^{-1} 3297 (NH), 2958, 2930 (CH), 1649 (CO), 1551, 1258, 1113 and 838; δ_H(300 MHz; $CDCl_3$) 0.046 (6 H, s, $SiMe_2$), 0.881 (9 H, s, Bu^{t}Si), 0.902 (3 H, d, *J* 6.4, Me), 0.912 (3 H, d, *J* 5.1, Me), 0.940 (3 H, d, *J* 5.0, Me), 0.950 (3 H, d, *J* 6.3, Me), 1.78–2.03 (4 H, m, $CHCH_2CH$, CH_2CHMe_2, $CHCHMe_2$), 3.543 (1 H, dd, *J* 3.7, ^2J −10.0, CH_AH_BO), 3.643 (1 H, dddd, *J* 2.8, 3.7, 6.1, 9.0, NCH), 3.731 (1 H, dd, *J* 2.8, ^2J −10.0, CH_AH_BO), 4.329 (1 H, dd, *J* 5.1, 9.5, BrCH) and 6.570 (1 H, d, *J* 9.0, NH); $\delta_C(CDCl_3)$ 168.62, 62.50, 56.23, 51.08, 44.98, 29.11, 26.47, 25.90, 22.72, 21.13, 21.09, 19.05, 18.23 and −5.48; *m/z* (EI) 396 ($MH^+ + 2$), 394 (MH^+), 380 ($M^+ + 2 - CH_3$), 378 ($M^+ - CH_3$), 352 ($M^+ + 2 - C_3H_7$), 350 ($M^+ - C_3H_7$), 338 ($M^+ + 2 - C_4H_9$) and 336 ($M^+ - C_4H_9$).

N-[(2R)-*Bromo*-4-*methylpentanoyl*]-L-*valinol* (**5**).—To a solution of *N*-[(2*R*)-bromo-4-methylpentanoyl]-*O*-(*tert*-butyldimethylsilyl)-L-valinol (0.6 g, 1.5 mmol) in methanol (15 cm^3) was added Amberlyst-15 (3 g) and the mixture stirred at room temperature for 2 h. The resin was filtered off, washed with methanol (10 cm^3) and the filtrate evaporated under reduced pressure. Chromatography on silica gel (ethyl acetate–hexane 30%, then ethyl acetate–hexane 50%) afforded compound **5** as a solid (0.38 g, 90%). M.p. 92–93 °C; $[\alpha]_D^{20}$ +2.5 (*c* 0.22, MeOH); TLC R_f 0.12 (ethyl acetate–hexane 30%); ν_{max}/cm^{-1} 3500–3100br (OH), 3420 (NH), 2960 (CH), 1654 (CO), 1560, 1458, 1388 and 1032; δ_H(200 MHz; $CDCl_3$) 0.89–0.99 (12 H, m, 4 Me), 1.77–1.97 (4 H, m, $CHCH_2CH$, CH_2CHMe_2, $CHCHMe_2$), 2.12 (1 H, br t, exch. D_2O, OH), 3.66–3.76 (3 H, m, CH_2O, NCH), 4.340 (1 H, dd, *J* 5.7, 9.1, BrCH) and 6.46 (1 H, br s, exch. CF_3CO_2D, NH); $\delta_C(CDCl_3)$ 170.05, 63.77, 57.65, 50.83, 44.82, 28.95, 26.45, 22.67, 21.02, 19.58 and 18.68; *m/z* (EI) 250 ($M^+ + 2 - CH_2OH$), 248 ($M^+ - CH_2OH$), 238 ($M^+ + 2 - C_3H_7$), 236 ($M^+ - C_3H_7$), 196 ($M^+ + 2 - CH_2OH - C_4H_8$) and 194 ($M^+ - CH_2OH - C_4H_8$).

(2S,5S)-2-*Isobutyl*-5-*isopropyl*-1,4-*oxazinan*-3-*one* (**6**).—Sodium hydride (0.072 g, 1.5 mmol; 50% in oil) was washed with hexane. The suspension was added to dry tetrahydrofuran (5 cm^3) under argon atmosphere. The alcohol **5** was added (0.38 g, 1.35 mmol), and the mixture stirred at room temperature for 2 h. Water and brine were added and the phases were separated. The aqueous layer was further extracted with ethyl acetate (10 cm^3). The organic extracts were combined and dried ($MgSO_4$) and evaporated to dryness under reduced pressure. Chromatography on silica gel (ethyl acetate–hexane 50%) afforded compound **6** as a white solid (0.24 g, 89%). M.p. 83–84 °C; $[\alpha]_D^{20}$ −16.6 (*c* 0.28, MeOH); TLC R_f 0.31 (ethyl acetate–hexane 50%); ν_{max}/cm^{-1} 3446 (NH), 3214 (NH), 2960 (CH), 1665 (CO), 1466, 1424, 1139 and 1108; δ_H(200 MHz; $CDCl_3$) 0.914 (3 H, d, *J* 6.2, Me), 0.933 (6 H, d, *J* 6.5, 2 Me), 0.972 (3 H, d, *J* 6.8, Me), 1.60–1.93 (4 H, m, $CHCH_2CH$, CH_2CHMe_2, $CHCHMe_2$), 3.070 (1 H, dddd, *J* 3.8, 4.0, 7.2, J_{NHCH} 3.7, NCH), 3.714 (1 H, dd, *J* 3.8, ^2J −12.1, CH_AH_BO), 3.760 (1 H, dd, *J* 4.0, ^2J −12.1, CH_AH_BO), 4.093 (1 H, dd, *J* 4.5, 8.8, OCH) and 6.00 (1 H, br s, NH); $\delta_C(CDCl_3)$ 172.15, 75.76, 63.39, 57.68, 39.93, 31.23, 24.42, 23.45, 21.29, 18.87 and 18.54; *m/z* (CI) 200 (MH^+), 156 ($M^+ - C_3H_7$) and 143 ($M^+ - C_4H_8$).

Boc-Val-ψ(CH$_2$O)Leu-OH (**2**).—Compound **6** (0.24 g, 1.2 mmol), was suspended in HCl (10 cm^3; 6 mol dm^{-3}) and the mixture was maintained under reflux for 20 h. The solution was evaporated under reduced pressure affording a solid which was dried overnight under high vacuum. The solid was suspended in dioxane–water (5%; 10 cm^3) and the pH of the solution was adjusted to 8–9 using triethylamine. Di-*tert*-butyl dicarbonate (0.30 g, 1.48 mmol) was added and the pH of the solution was maintained at 8–9 by addition of triethylamine. The reaction mixture was concentrated and rediluted with water. The mixture was extracted with diethyl ether (15 cm^3) and the extract was discarded. The aqueous phase was acidified to pH 2 with solid citric acid and extracted with ethyl acetate (2 × 25 cm^3). The combined organic extracts were dried ($MgSO_4$) and evaporated to dryness under reduced pressure. Chromatography on silica gel (ethyl acetate–hexane 20% + 0.5% acetic acid) afforded compound **2** as a white solid (0.23 g, 60%). M.p. 115.5–116 °C (hexane); $[\alpha]_D^{20}$ −66.4 (*c* 1.08, MeOH); TLC R_f 0.17 (ethyl acetate–hexane 20% + 0.5% acetic acid); ν_{max}/cm^{-1} 3363 (NH), 2958 (CH), 1733 (CO), 1663 (CO), 1539, 1367, 1207, 1175, 1133 and 1117; δ_H(200 MHz; $CDCl_3$) 0.910 (12 H, m, 4 Me), 1.42 (9 H, s, Bu^t), 1.51–1.85 (4 H, m, $CHCH_2CH$, CH_2CHMe_2, $CHCHMe_2$), 3.48–3.57 (3 H, m, NCH, OCH_2), 3.90 (1 H, dd, *J* 8.6, 4.4, OCH) and 4.72 (1 H, br s, NH); $\delta_C(CDCl_3)$ 177.33, 156.67, 79.46, 77.99, 71.59, 55.79, 41.61, 29.33, 28.36, 24.52, 23.15, 21.58, 19.53 and 18.72; *m/z* (CI) 318 (MH^+), 274 ($M^+ - C_3H_7$), 262 ($MH^+ - C_4H_8$), 244 and 218 (Found: MH^+, 318.2278. Calc. for $C_{16}H_{32}NO_5$: *M*, 318.2280).

X-Ray Crystal Structure Determination of **1** *and* **2**.—Prismatic crystals of **1** were obtained by slow evaporation of a diethyl ether solution at room temperature. Prismatic crystals of **2** were obtained by slow cooling to room temperature of a hot hexane solution. For both structures the NRCCAD programs[10] were used for centring, indexing and data collection. The unit cell dimensions were obtained by a least-squares fit of 24 centred reflections in the range of $60° < 2\theta < 80°$. Reflections were measured with a constant scan speed of 2.7° min^{-1}. During data collection, the intensities of 2 standard reflections were monitored every 60 min. No significant decay was observed. Intensity data were collected on an Enraf-Nonius CAD-4 automatic diffractometer. Details of crystal data and data collection are given in Table 1. Both structures were solved by the application of direct methods and refined by full matrix least squares using the NRCVAX program.[11] Weight based on counting statistics were used. A secondary extinction coefficient was included in the refinement,[12] the final values were 1.38(7) and 0.47(3) μm for **1** and **2** respectively. Atomic scattering

Table 1 Crystal data and details of structure determination for compounds **1** and **2**

	Crystal data	
	1	**2**
Formula	$C_{16}H_{30}N_2O_5$	$C_{16}H_{31}NO_5$
M	330.43	317.43
System	Orthorhombic	Monoclinic
Space group	$P22_12_1$[18]	$P2_1$[4]
a/Å	10.9546(3)	6.0341(10)
b/Å	18.4044(3)	15.3457(16)
c/Å	20.4474(7)	10.6308(11)
β(°)	—	101.064(11)
V/Å^3	4122.5(2)	966.09(21)
Z	8	2
D_{calc}/g cm^{-3}	1.065	1.089
$F(000)$/e$^-$	1440	346
μ(Cu-Kα)/cm^{-1}	0.61	0.62
Crystal size/mm	0.20 × 0.15 × 0.10	0.25 × 0.25 × 0.35
Data collection		
T/K	293	213
Radiation	Cu-Kα	Cu-Kα
θ(min–max)/(°)	1.0, 71.7	1.0, 71.7
Scan type	$\omega/2\theta$	$\omega/2\theta$
Scan (°)	1.0 + 0.14 tan(θ)	1.0 + 0.14 tan(θ)
Dataset	0:13; 0:22; 0:25	−7:7; 0:18; 0:13
Total uniq. data	4496	1974
Observed reflection	2189 [$I > 2.0\,\sigma(I)$]	1880 [$I > 2.5\,\sigma(I)$]
Refinement		
N_{ref}, N_{par}	2189, 408	1880, 199
R, R_w	0.068, 0.061	0.039, 0.040
GoF	2.41	3.41
Max. shift/error	0.104	0.001
Min. res. dens./e$^-$ Å^{-3}	−0.16	−0.20
Max. res. dens./e$^-$ Å^{-3}	0.27	0.22

factors stored in the NRCVAX program were those of Cromer and Waber.[13] Hydrogen atomic positions were calculated for **1** and **2** but not refined for **1**. An orientation disorder on the Val side chain was found in one of the independent molecules of **1** (**1b**), the occupancy refinement showed a 50:50 ratio. Both orientations were refined using rigid bond lengths and angles set at 1.54 Å and 109°, high thermal motion prevented conservation of good geometry. All non-hydrogen atoms were set anisotropic for refinement except for C(11) in **1a** and C(10'), C(11') and C(12') in **1b**. Details of structures refinement are given in Table 1.*

NMR Solution Study of **1** *and* **2**.—Solutions 0.015 mol dm^{-3} of **1** or **2** in [$^2H_6$]DMSO were degassed by two cycles of successive freezing and pumping under high vacuum. The NMR tubes were filled with Argon and sealed. 1D And 2D spectra were recorded with a Brüker AC-F 300 HC spectrometer operating at 300.13 MHz for ^{1}H and equipped with a BVT-1000E variable temperature controller.† 1D Normal and selective proton decoupled spectra were recorded with 32 K data points. The FIDs were zero filled to 64 K data points and resolution enhanced by multiplication with a gaussian function having its maximum at 0.3 s.

Assignment of the 1D spectra was performed by selective proton decoupling and multiplicity analysis. One difficulty was however encountered: Leu C$^\gamma$H and Val C$^\beta$H were overlapping in compound **2** which precluded the assignment of the methyl resonances by selective irradiation. A 2D relayed coherence transfer experiment[14] (which allowed the observation of ^4J cross-peaks) indicated a correlation between Val C$^\alpha$H and the two doublets at around 0.79 ppm, no cross-peaks were detected with the two doublets around 0.86 ppm. This was further checked by irradiating the two doublets around 0.86 ppm (sufficiently separated from those at 0.79 ppm) which resulted in the collapse of the Leu C$^\gamma$H resonance to a doublet of doublets at 1.746 leaving the Val C$^\beta$H multiplet (a quasi octuplet) intact. Similarly when the two doublets around 0.79 ppm were irradiated, the Val C$^\beta$H resonance collapsed to a doublet at 1.707 ppm leaving the Leu C$^\gamma$H complex multiplet at 1.746 ppm intact. Accurate determination of chemical shifts and coupling constant for complex and second order spin system was performed with the PANIC simulation program. Spin systems were reduced to the minimum number of nuclei by suitable selective proton decoupling in order to minimize the number of parameters to be optimized in the simulation. Once the chemical shifts and coupling constants were determined for the proton selective decoupled spectra, the undecoupled spectra were analysed using the previous values as starting parameters.

2D NOE spectra were recorded at 296.0 K using the standard sequence of three 90° pulses. A relaxation delay of 3 s was used. The experiment was repeated with two different mixing times (0.3 and 0.5 s). In each experiment, the mixing time was randomly varied by ±4% in order to strongly reduce the J scalar crosspeaks.[15] Minimal spectral widths were used. 1 K Data points were acquired in F2 dimension and 128 t_1 in F1. 32 Transients were accumulated for each t_1. The increments for the t_1 values were 418 μs with **1** and 452 μs with **2**, and the initial t_1 value was 3 μs. Zero filling was accomplished in F1 before 2D Fourier transformed. This resulted in a digital resolution of 4.67 Hz/point with **1** and 4.32 Hz/point with **2**. The 2D spectra were symmetrized. NOE crosspeak intensities and positions were estimated from cross sections taken at maximum diagonal peak intensity. Relative cross-peaks intensity were similar for experiments conducted with mixing time of 0.3 or 0.5 s but were significantly less intense with the shorter mixing time. Due to important t_1 noise at the Bu^t resonance, cross-peaks found at this position were not considered. Cross-peaks that were too close to the diagonal peaks were also not considered.

Molecular Modelling Study of **1** *and* **2**.—Input structures for the molecular modelling study were based on solid-state coordinates of **1a** and **2**. Hydrogen atoms were added at ideal geometric locations. Molecule **1a** was minimized using MAXIMIN2 until the convergence criteria of 0.001 kcal mol^{-1} was reached in order to reduce small distortions resulting from thermal motion in the crystal (*vide supra*). For each molecule, the SEARCH module of SYBYL[16] was used to explore the allowed conformations by systematically varying the torsional angles with specified increments. φ,ψ-Backbone torsional angles (as defined in Table 2),‡[17] were varied from 0 to 360° by 20° increments. Side chain torsional angles Val $\chi^{1,1}$ and Leu $\chi^1,\chi^{2,1}$ were varied to adopt values of 60 ± 10°, −60 ± 10° and 180 ± 10°. The amide and urethane torsional angle ω and ω_0 were held fixed at their crystal structure values. In the case of compound **2**, the ω' torsional angle was first fixed at the crystal structure value but the SEARCH procedure was repeated with ω' adopting dihedral angle value of +60° and −60°. Rigid bond lengths and bond angles were assumed during the SEARCH process. A general cut-off of 0.85 times the

* Atomic coordinates, bond lengths, bond angles and thermal parameters have been deposited at the Cambridge Crystallographic Data Centre; for details see 'Instructions for Authors', *J. Chem. Soc., Perkin Trans. 2*, 1994, issue 1.

† 1D And 2D spectra, have been desposited under the Supplementary Publications Scheme; for details see 'Instructions for Authors', *J. Chem. Soc., Perkin Trans. 2*, 1994, issue 1 [Supp. Pub. No. 57013 (5 pp.)].

‡ The principal dihedral angles are used unless otherwise stated.

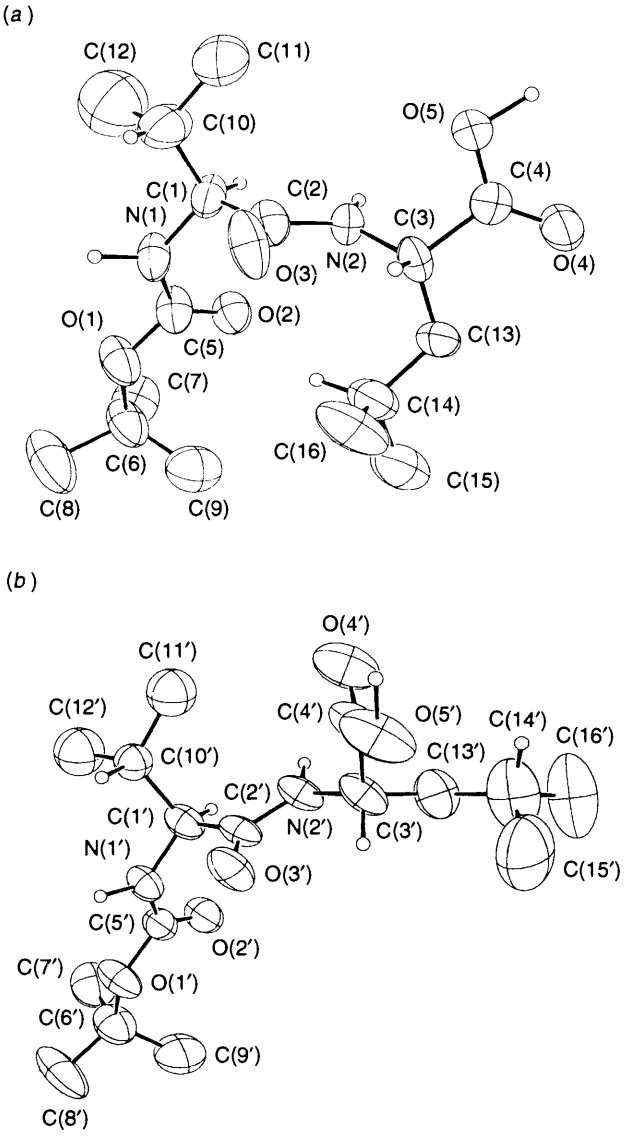

Fig. 1 ORTEP plot and atoms numbering of the two independent molecules of **1** oriented such that the Boc-Val moiety coincided [**1a** (*a*); **1b** (*b*)]. For clarity, the hydrogen atoms on the methyl and the methylene have been omitted and only one rotamer for Val is depicted for **1b**.

van der Waals radius served to reject conformations with bad atomic contact.[18] For each allowed conformation, the conformational energy was computed. This energy was calculated using the molecular mechanic approach using the standard parameters of the Tripos force field. An electrostatic contribution was included. The partial atomic charges were computed on the initial conformation from a Mulliken population analysis of molecular orbital calculations using the AM1 Hamiltonian (MOPAC).[19] All computations were performed on an IBM RISC 6000 model 320H, each search requiring about 2.5 h of CPU time. The results are illustrated in the form of Ramachandran plot for each pair of φ,ψ-backbone torsional angles. Conformations that were within 10 kcal mol^{-1} of the global minimum energy were included in the map. The side chain conformations that led to the minimum energy for a particular φ,ψ values were used for plotting the maps.

Results

X-Ray Molecular Conformations.—A view of the crystal structure and atomic numbering of Boc-Val-Leu-OH (**1**) and

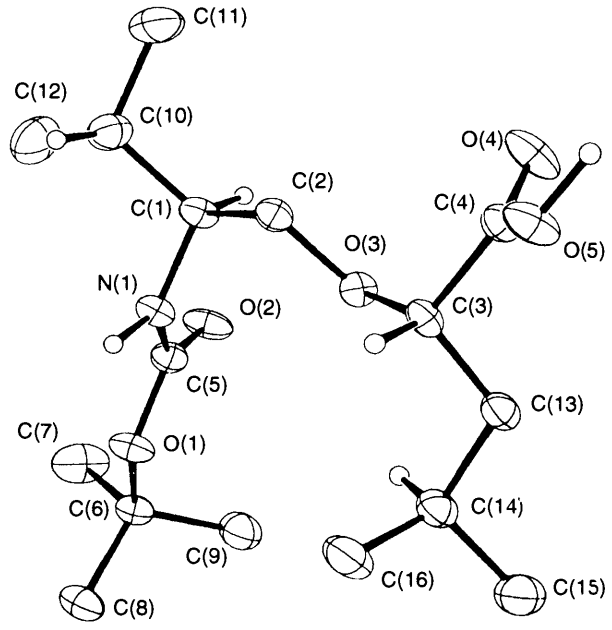

Fig. 2 ORTEP plot and atoms numbering of **2** oriented such that the Boc-Val moiety coincided with that depicted for **1**. For clarity, the hydrogen atoms on the methyls and the methylene have been omitted.

Boc-Val-ψ(CH_2O)-Leu-OH (**2**) is shown in Figs. 1 and 2 respectively. Table 2 provides selected comparative torsional angles.

The crystal structure of **1** consists of two independent molecular conformations, **1a** and **b**, which differ mainly in the Leu side chain conformation. The Leu side chain adopts the g^-t conformation (defined by χ^1 and $\chi^{2,1}$ dihedral angles) in **1a** while it is found in the tg^+ conformation in **1b**. It is noteworthy that the Leu side chain conformation observed in **1a** is the one most frequently found in reported crystal structures while the other (tg^+) is the next frequently observed; all other conformations being rarely reported.[20] As a result of these two different side chain conformations, the crystal structure **1a** is compact and characterized by a short C(9)–C(16) distance [4.775(12) Å] compared to **1b** which has a longer C(9)–C(16) distance [9.597(15) Å].

The Val side chain conformation as defined by the principal dihedral angle $\chi^{1,1}$ is found in the *t* rotameric state in **1a** while both the *t* and g^- rotamers are observed in structure **1b** in approximately equal population. It has been reported that the *t* rotamer occurs most often in the Val residue incorporated in peptides (50%) while each of the two others (g^+ and g^-) were equally populated (25%) in the crystal structures.[20] The occurrence of the g^- rotamer for the Val side chain is usually associated with a local ψ dihedral angle value of 155° ± 10°[20] as is the case in structure **1b**.

In both conformations, the amide bond adopts the usual *trans* configuration with a deviation from 180° of 8° and 2° for **1a**, and **b** respectively. The *N*-Boc urethane group was also observed in the *trans* configuration (dihedral angle ω_0).[21] It is noteworthy that the urethane bond was observed in the *cis* configuration in the reported crystal structure of Boc-Val-OH.[22]

The crystal structure of Boc-Val-ψ(CH_2O)-Leu-OH consists of only one molecular conformation which is similar to the compact structure of **1a**. The Leu and Val side chains adopt the same conformation as was found in **1a** and similarly the atoms C(9) and C(16) are close [5.060(6) Å]. The dihedral angle ψ_{Val} and φ_{Leu} values show significant departure from the values observed in **1a** or **b** and this can be a consequence of the surrogate CH_2–O group. The dihedral angle ψ_{Val} value of

Table 2 Selected torsional angles (°) for **1** and **2**

	Angle	**1a**	**1b**	**2**
Boc				
C(6)–O(1)–C(5)–N(1)	θ_1	−177.1(7)	168.8(7)	178.1(3)
O(1)–C(5)–N(1)–C(1)	ω_0	174.2(7)	175.6(7)	172.9(3)
Val[1]				
C(5)–N(1)–C(1)–C(2)	φ	−82.4(6)	−100.9(6)	−121.7(3)
N(1)–C(1)–C(2)–N(2)	ψ	121.0(7)	149.6(7)	58.3(2)
C(1)–C(2)–N(2)[a]–C(3)	ω,ω'[c]	−172.1(7)	178.1(7)	−165.7(3)
N(1)–C(1)–C(10)–C(11)	$\chi^{1,1}$	179.8(9)	175.2(11)[b]	−174.7(4)
N(1)–C(1)–C(10)–C(12)	$\chi^{1,2}$	−64.9(7)	−62.1(8)[b]	−51.7(2)
Leu[2]				
C(2)–N(2)–C(3)–C(4)	φ	−133.2(6)	−99.2(6)	−68.3(2)
N(2)–C(3)–C(4)–O(4)	$\psi_T{}^1$	−139.3(7)	−46.0(5)	−28.4(2)
N(2)–C(3)–C(4)–O(5)	$\psi_T{}^2$	42.7(4)	138.9(8)	152.2(3)
N(2)–C(3)–C(13)–C(14)	χ^1	−62.6(5)	179.2(9)	−56.8(2)
C(3)–C(13)–C(14)–C(15)	$\chi^{2,1}$	170.8(8)	52.5(7)	−179.3(3)
C(3)–C(13)–C(14)–C(16)	$\chi^{2,2}$	−66.5(6)	178.5(10)	−55.4(2)

[a] Atom N(2) in **1** corresponds to O(3) in **2**. [b] $\chi^{1,1}$ and $\chi^{1,2}$ take the values −56.2(9) and 59.3(9) respectively in the other rotamer. [c] For distinction, the designation ω' was used for this torsional angle for compound **2**.

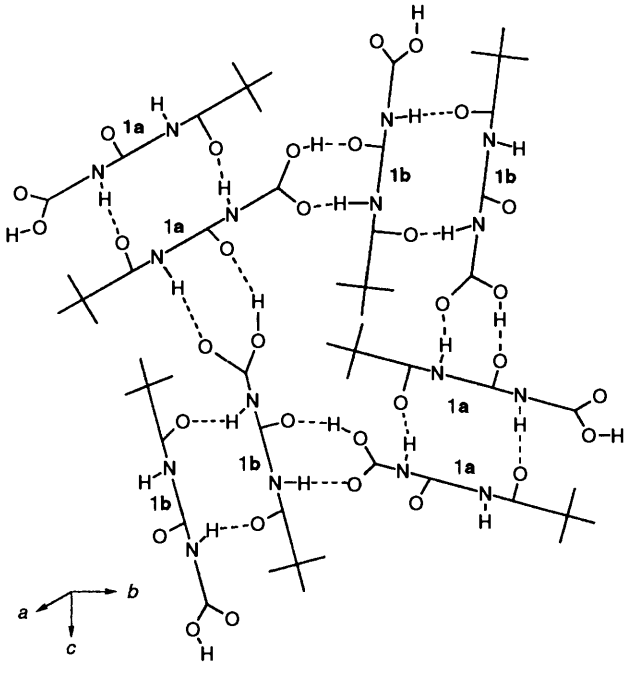

Fig. 3 Schematic representation of the hydrogen bonding network involved in the crystal packing of **1**

58.3(2)° is probably a consequence of minimizing 1–4 interactions between Val C^β and the ether oxygen [torsional angle C(10)–C(1)–C(2)–O(3) = −178.7(3)°]. Similarly, the dihedral angle φ_{Leu} value of −68.3(2)° is probably a consequence of minimizing 1–4 interactions between Leu C^β and the surrogate methylene [torsional angle C(2)–O(3)–C(3)–C(13) = 171.4(3)°].

The ω' torsional angle assumes a value of −165.7(3) in compound **2**. It clearly adopts a *trans* orientation, although with larger deviation from 180° than the unstrained *trans* amide bond. Closer examination of the surrogate geometry compared to the amide reveals that: (*i*) the C(1)–C(2) bond length remains essentially the same for both compounds; (*ii*) the CH_2–O bond is 0.09 Å longer than the average amide bond [C(2)–N(2)]; (*iii*) the O–C^α bond is 0.04 Å shorter than the average C′–C^α bond [C(3)–N(2)]. Valence angles around C(1) and C(3) were not significantly different between **1** and **2** except for C(2)–C(1)–C(10) which was larger in the surrogate compound **2**. As a consequence of the tetrahedral nature of the atoms forming the methylene–oxy bond and to the quite short $C(sp^3)$–$O(sp^3)$ bond, the C^α_i–C^α_{i+1} distance is 0.12 Å shorter in the pseudopeptide compared to the regular peptide: 3.667(4) Å in **2**, 3.806(8) Å in **1a** and 3.762(9) Å in **1b**. In molecule **2**, the urethane group adopt the *trans* configuration and the Boc group geometry is in agreement with reported mean values.[21]

X-Ray Molecular Packings.—In the crystal of **1** all potential hydrogen bonding donors and acceptors are involved in intermolecular hydrogen bonds. Fig. 3 shows schematically the hydrogen-bond network for compound **1** and Table 3 gives the respective hydrogen bond geometries. Each independent molecule is hydrogen-bonded with a two-fold related molecule through the amide N(2)H. These hydrogen bonds are oriented in the direction of the *c* crystallographic axis for **1a** and in the *b* crystallographic axis for **1b**. The two-fold related dimers are hydrogen-bonded to their corresponding independent molecule in both *b* and *c* crystallographic axis direction. The hydrogen bonds are ensured through the carboxylic group of **1a** in the *b* direction [O(5)H and O(4)], and through the carboxylic group of **1b** in the *c* direction [O(5)H′ and O(4)′]. Such a hydrogen bonding scheme gives rise to layers of molecules parallel to the *bc* plane. The packing along *a* is achieved through van der Waals interactions with the Val or Leu side chain and the *tert*-butyl group.

Crystal packing is quite different in compound **2** owing to the absence of the N(2)H donor. The hydrogen bonding pattern is a more typical head-to-tail network.[23] The terminal carboxylic group is hydrogen-bonded to the head of two molecules. O(4) Accepts the hydrogen from urethane N(1)H of a molecule related by translation along *a* while O(5)H donates to O(2) of a molecule related by the two-fold screw axis (Table 3). This gives rise to an infinite network of hydrogen bonds in the *ab* crystallographic plane. As is the case of **1**, the cohesion in *c* direction is ensured by van der Waals interactions involving the hydrophobic Val and Leu side chain and the *tert*-butyl group.

Solution Conformation.—Table 4 shows the ^1H assignment of NMR spectra of compounds **1** and **2** in [$^2H_6$]DMSO at 296.0 K. The presence of about 10% of *cis* urethane bond (ω_0) was detected for compounds **1** and **2** at 296 K in [$^2H_6$]DMSO. This phenomenon has been frequently encountered in Boc-amino-acids[24] owing to the small energy difference between the

Table 3 Intermolecular hydrogen bond distances and angles for compounds **1** and **2**

D[a]	A[b]	d(D···A)/Å	θ(D–H···A)/(°)	Symmetry[c]
1				
N(1)H	O(4′)	3.048(7)	146[d]	(x, y, z)
N(2)H	O(2)	2.993(6)	170[d]	$(x, -y, 2 - z)$
O(5)H	O(3′)	2.651(6)	163[d]	$(-x, \frac{1}{2} - y, \frac{1}{2} + z)$
N(1)H′	O(4)	2.921(6)	155[d]	$(-x, \frac{1}{2} - y, -\frac{1}{2} + z)$
N(2)H′	O(2′)	2.920(6)	170[d]	$(x, -y, 1 - z)$
O(5)H′	O(3)	2.576(6)	157[d]	(x, y, z)
2				
N(1)H	O(4)	2.969(4)	147(2)	$(-1 + x, y, z)$
O(5)H	O(2)	2.633(3)	156(3)	$(2 - x, \frac{1}{2} + y, 1 - z)$

[a] Donor. [b] Acceptor. [c] Of atom A. [d] Hydrogen atom positions were calculated but not refined.

Table 4 ^{1}H NMR data for **1** and **2** (300 MHz, [$^2H_6$]DMSO, 296.0 K)

	$\delta(\pm 0.001)/J(\pm 0.02)$/Hz	
	1	**2**[a]
Boc	1.363	1.361
Val		
δ_{NH}	6.638	6.525
$J_{NH-C^{\alpha}H}$	9.18	9.12
$\delta_{C^{\alpha}H}$	3.765	3.358
$J_{C^{\alpha}H-C^{\beta}H}$	7.32	6.09
$\delta_{C^{\beta}H}$	1.906	1.707
$J_{C^{\beta}H-Me^{\gamma}{}_A}$	7.04	6.91
$J_{C^{\beta}H-Me^{\gamma}{}_B}$	6.74	6.85
$\delta_{Me^{\gamma}{}_A}$	0.840	0.807
$\delta_{Me^{\gamma}{}_B}$	0.803	0.780
Leu		
δ_{NH}	7.968	—
$J_{NH-C^{\alpha}H}$	7.92	—
$\delta_{C^{\alpha}H}$	4.224	3.764
$J_{C^{\alpha}H-C^{\beta}H_A}$	9.78	9.65
$J_{C^{\alpha}H-C^{\beta}H_B}$	5.26	3.95
$\delta_{C^{\beta}H_A}$	1.536	1.499
$\delta_{C^{\beta}H_B}$	1.477	1.367
$J_{C^{\beta}H_A-C^{\gamma}H}$	4.66	4.72
$J_{C^{\beta}H-C^{\gamma}H}$	8.75	8.67
$J_{C^{\beta}H_A-C^{\beta}H_B}$	−13.61	−13.99
$\delta_{C^{\gamma}H}$	1.650	1.746
$J_{C^{\gamma}H-Me^{\delta}{}_A}$	6.57	6.57
$J_{C^{\gamma}H-Me^{\gamma}{}_B}$	6.52	6.70
$\delta_{Me^{\delta}{}_A}$	0.874	0.874
$\delta_{Me^{\delta}{}_B}$	0.812	0.862

[a] δ_{CH_A-O} 3.532, δ_{CH_B-O} 3.146, $J_{C^{\alpha}H-CH_A-O}$ 4.80, $J_{C^{\alpha}H-CH_B-O}$ 7.05, $J_{CH_A-CH_B}$ −9.35.

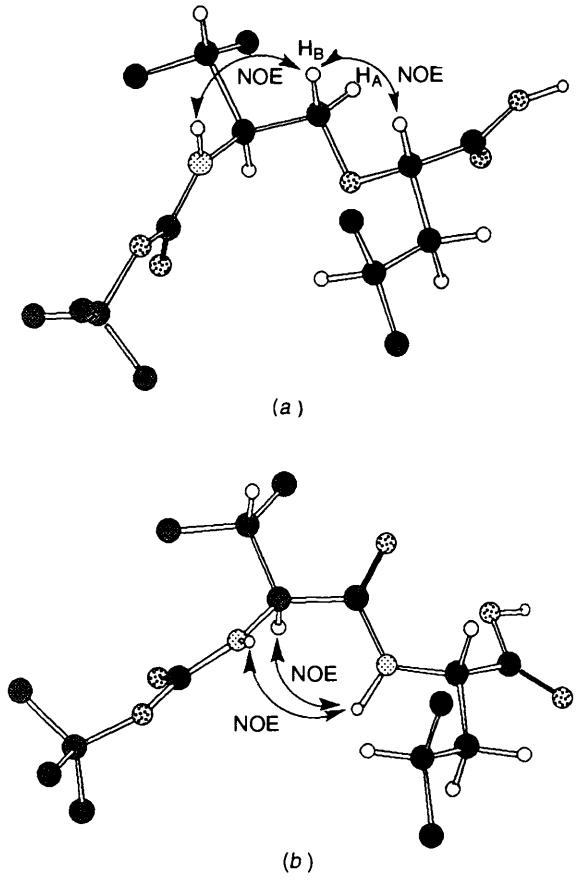

Fig. 4 Most probable solution conformation for **2** (*a*) and **1** (*b*) that are consistent with NMR data in [$^2H_6$]DMSO. The most intense NOEs observed inside the backbone are shown with an arrow.

cis–trans urethane configurations. Consequently, an exchange cross-peak was observed between the downfield *trans* urethane NH and the upfield *cis* urethane NH in the 2D NOE spectra.

According to the NMR data, the $\psi(CH_2O)$ pseudodipeptide (**2**) seems to have a backbone conformational preference in solution that is related to the crystal structure. A strong NOE cross-peak was observed between Val NH and the upfield diastereotopic methylene-oxy proton CH_B–O while only a weak signal was detected with CH_A–O. Moreover, CH_B–O experiences stronger NOE with Leu C$^{\alpha}$H than CH_A–O does. Taken together with the fact that $J_{C^{\alpha}H-CH_B-O}$ is significantly greater than $J_{C^{\alpha}H-CH_A-O}$ which stems from a preferred *trans* orientation of CH_B–O relative to Val C$^{\alpha}$H,*[,25] and that the Bystrov relationship suggests values of −100° or −140° for the φ_{Val} dihedral angle,[26] the crystal conformation may indeed represent the most preferred conformation of **2** in solution. Fig. 4(*a*) shows a probable conformation of **2** that may explain the preceding observations. Close examination of Fig. 4(*a*) reveals that the diastereotopic CH_A–O lies on the same side as the carboxylic group which may explain its deshielding compared to CH_B–O.

Free rotation probably occurs for the Val side chain of **2** owing to the value of $J_{CH^{\alpha}CH^{\beta}}$ and to the strong NOE detected

* Rotamer population analysis around N–C–C–O using Pachler's approach with parameters derived by Abraham and Gatti provided 49% for the g^+ rotamer (the crystallographic one), 33% for the *t* and 19% for the *g*

between Val NH and Val Mes which is indicative of the occurrence of g^+ or g^- rotamers for this side chain.*

The important chemical shift differences between the Leu geminal diastereotopic $C^{\beta}H_2$ ($\Delta\delta = 0.13$ ppm) along with their considerable difference in vicinal coupling with Leu $C^{\alpha}H$ and $C^{\gamma}H$ ($\Delta J = 4$–6 Hz) indicates conformational homogeneity[27] for the Leu side chain. Assuming that the large coupling constant values are associated with preferred *trans* orientation for the involved protons and that the small coupling constants are associated with a *gauche* orientation, two side chain conformations for Leu are possible. Fig. 5 shows Newman projections of the two possible side chain conformations. Expressed as their principal dihedral angles (χ^1 and $\chi^{2,1}$) they correspond to the g^-t and tg^+ conformations. As mentioned above these are the two most often occurring side chain conformations cited for Leu and it is not possible to reject one of them on the basis of unfavourable steric interactions. It is also not possible to reject one of them on the basis of presence or absence of NOE (since the usual NH is replaced by O). Interestingly, the diastereotopic H^{β} which is *trans* relative to H^{α} can be expected to be more deshielded compared to the one which is *gauche* relative to H^{α} (Fig. 5); this is indeed the case (Table 4).

The important NOE observed between Val-NH and Leu-NH for compound **1** is indicative of a solution backbone conformation in [$^2H_6$]DMSO that departs from the backbone crystal structure where the two NHs were pointing in opposite directions. Furthermore this is accompanied by a very strong NOE between Val-$C^{\alpha}H$ and Leu-NH (CH_iNH_{i+1}). These observations along with the fact that the value of Val J_{NHCH} is quite high suggests values of $-150°$ and 60° for Valφ,ψ dihedral angles respectively as depicted in Fig. 4(*b*). The possible existence of a stable C_{eq}^7 intramolecular hydrogen bond between the urethane carbonyl and Leu-NH, although not supported from NOE data, was investigated by studying the temperature effect on the NH chemical shift in [$^2H_6$]DMSO ($\Delta\delta/\Delta T$). A constant slope of -5.1 ppb K^{-1} was obtained between 296 and 346 K which rules out the presence of this intramolecular hydrogen bond in solution.

Similar to compound **2**, the Val side chain of **1** is free to rotate owing to the typical J_{AV} value observed for $J_{C^{\alpha}HC^{\beta}H}$. The Leu H^{β}s are diastereotopic in compound **1** but the chemical shift difference is smaller than observed with compound **2**. The coupling constants involving the Leu side chain protons suggest the same possible side chain conformation described for **2** (Fig. 5). The observation of a small NOE between Leu-NH and Leu-$C^{\gamma}H$ suggests that the g^-t conformation may be dominant in solution.

* The X-ray diffraction study of **2** was first conducted at room temperature but the high thermal motion associated with the Val side chain prevented the obtention of good R even with rigid body refinement and attempt to localize other rotamers by Fourier difference. The experiment was then conducted at 213 K.

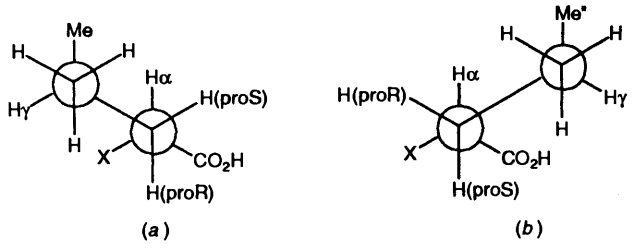

Fig. 5 Newman projection illustrating the relationship between protons for the two possible Leu side chain conformations in solution: (*a*) $\chi^1,\chi^{2,1} = g^-t$; (*b*) $\chi^1,\chi^{2,1} = tg^+$. Compound **1**, X = NH; **2**, X = O.

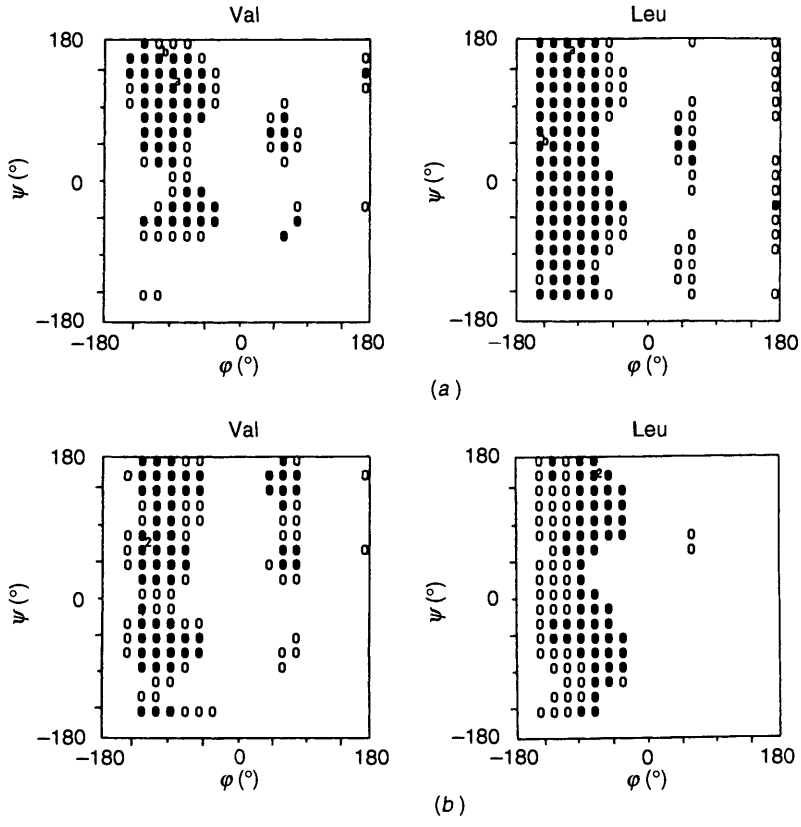

Fig. 6 Ramachandran maps (φ,ψ) for the Val and Leu residue for (*a*) **1** and (*b*) **2** obtained by systematic conformational search. The full dots represents conformations that were within 5 kcal mol^{-1} of the global energy minimum, the empty dot represents conformations that were between 5 and 10 kcal mol^{-1} of the global energy minimum. The small letters a and b in (*a*) indicate the φ,ψ values observed for **1a** and **b** respectively in the crystal state. The small number 2 in (*b*) indicates the φ,ψ values observed in the crystal state.

Conformational Mimicry.—Ramachandran maps obtained for both compounds are depicted in Fig. 6. The maps depicted for compound **2** are with the ω' torsional angle fixed at the crystallographic value. When the systematic SEARCH was conducted with ω' torsional angle fixed at $+60°$ or $-60°$, the allowed conformations were more than 7 kcal mol^{-1} higher in energy compared to the minimum energy conformation obtained using ω' fixed at $-166°$. Moreover, the plot of Ramachandran map in this case (data not shown) revealed only a narrow populated area. The severe *gauche* steric interactions that occur between the two tertiary C^{α}s when $\omega' = +60°$ or $-60°$ could account for the higher conformational energies obtained in these runs. The resulting low population and high steric energy of *gauche* rotamers for the ω' torsional angle is further supported by our NOE measurements since no NOE was detected between the two $C^{\alpha}Hs$ for **2** which should have been observed otherwise.

Comparison of the Ramachandran maps for the Val residue in **1** and **2** shows that the number of allowed conformations is larger for the pseudodipeptide. The replacement of the carbonyl by a methylene increased the number of values available to ψ, particularly for the negative values of ψ. Rotation around ψ_{Val} for **2** is indeed well represented by a three-fold rotational barrier with three low energy minima at 60°, $-60°$ and 180°.

On the other hand, the Ramachandran maps of the Leu residue show that the number of allowed conformations within 5 kcal mol^{-1} for **2** is smaller compared to **1**; the replacement of the amide NH by an oxygen reduced the number of φ_{Leu} values available. The preferred φ_{Leu} values are concentrated around $-60° \pm 30°$ in **2** while values from $-60°$ to $-180°$ were allowed within 5 kcal mol^{-1} for **1**. As mentioned earlier, the preferred dihedral angle value for φ_{Leu} stems from a tendency to minimize unfavourable interactions between Leu-C^{β} and -CH_2 which are amplified owing to the short $C(sp^3)$–$O(sp^3)$ bond length.

Discussion

Owing to the double bond character of the native amide, this structural element is recognized as of prime importance in the elaboration of the three dimensional conformation of polypeptide chains. It is well known that peptide bonds usually do not deviate from planarity by more than 24°.[28] The substitution of an amide bond by a methylene-oxy group within peptide structures would be expected to introduce substantial rotational flexibility. Our experiments demonstrate that the methylene-oxy surrogate confers unexpected rigidification factors in a model hydrophobic dipeptide.

The X-ray crystal structure of **2** and the molecular modelling study revealed a preferred *trans* orientation for the C–C–O–C bond (where C is an sp^3 carbon). In the pseudopeptide context it directs the preferred values of both the ω'_i and φ_{i+1} torsional angles. This is corroborated by a previous study on oxo-crown ethers which have demonstrated the antipathy for *gauche* orientation of the C–C–O–C bond.[29] This is at variance with the C–C–S–C bond (where C is an sp^3 carbon) which have been shown to adopt a *gauche* orientation in thia-crown ether.[29] This reversal of preference has been explained in terms of favourable or unfavourable 1–4 *gauche* interactions. Owing to the short C–O bond length in the sequence C–C–O–C the 1–4 *gauche* interacts are unfavourable while in the C–C–S–C sequence the long C–S bond renders the 1–4 *gauche* interactions favourable. Recently, the crystal structural of Boc-Ala-$\psi(CH_2S)$-Phe-OH has been reported[30] and indeed the ω' angle adopts a value of $-71°$.

Our NMR study suggests that the preferred backbone conformation of **2** in DMSO solution might be closely related to its crystal structure conformation and gives support that an unexpected rigidification element is introduced by the methylene-oxy surrogate.

In summary, owing to internal conformational constraints, the methylene-oxy surrogate adopts a preferred orientation similar to the *trans* amide bond and causes the φ_{i+1} torsional angle to adopt a preferred value of $-60°$. Based on molecular mechanic calculation, the replacement of the carbonyl by a methylene group allows, however, more rotational flexibility for ψ_i. The ether oxygen is a weak hydrogen bond acceptor and alteration in biological activity upon substitution with this surrogate can be associated with a loss of a hydrogen bond donor or acceptor involved in a crucial interaction with a receptor macromolecule, although the conformational effects (*vide supra*) must also be taken into account.

Acknowledgements

G. V. thanks NSERC for a doctoral scholarship. Our thanks also go to Gaston Boulay for mass spectrometry measurements and to Françoise Sauriol and Normand Pothier for judicious advice in NMR spectroscopy.

References

1 For recent reviews, see J. Rizo and L. M. Gierasch, *Ann. Rev. Biochem.*, 1992, **61**, 387; A. Giannis and T. Kolter, *Angew Chem., Int. Ed. Engl.*, 1993, **32**, 1244.
2 J. DiMaio and P. W. Schiller, *Proc. Natl. Acad. Sci. USA*, 1980, **77**, 7162.
3 For example, see G. Villeneuve, J. DiMaio, T. H. Chan and A. Michel, *J. Chem. Soc., Perkin Trans. 1*, 1993, 1897.
4 For review, see D. T. Elmore, *Amino Acids Pept.*, 1991, **22**, 83.
5 For example, see M. C. Allen, W. Fuhrer, B. Tuck, R. Wade and J. M. Wood, *J. Med. Chem.*, 1989, **32**, 1652; J. F. Dellaria, R. G. Maki, H. H. Stein, J. Cohen, D. Whittern, K. Marsh, D. J. Hoffman, J. J. Plattner and T. J. Perun, *J. Med. Chem.*, 1990, **33**, 534.
6 A. F. Spatola, A. L. Rockwell and L. M. Gierasch, *Biopolymers*, 1983, **22**, 147; M. Goodman, *Biopolymers*, 1985, **24**, 137; B. Hassan and M. Goodman, *Biochemistry*, 1986, **25**, 7596; N. J. Mammi and M. Goodman, *Biochemistry*, 1986, **25**, 7607; A. F. Spatola, M. K. Anwer, A. L. Rockwell and L. M. Gierasch, *J. Am. Chem. Soc.*, 1986, **108**, 825; P. Van der Elst, M. Elseviers, E. DeCock, M. Van Marsenille, D. Tourwé and G. Van Binst, *Int. J. Peptide Protein Res.*, 1986, **27**, 633; G. Zanotti, C. Toniolo, T. J. Owen and A. F. Spatola, *Acta Crystallogr., Sect. C*, 1988, **44**, 1576; C. Tonolio, G. Valle, M. Crisma, J. S. Kaltenbronn and J. T. Repine, *Peptide Res.*, 1989, **2**, 332; C. Toniolo, *Biopolymers*, 1989, **28**, 247; D. B. Sherman and A. F. Spatola, *J. Am. Chem. Soc.*, 1990, **112**, 433; M. K. Anwer, D. B. Sherman and A. F. Spatola, *Int. J. Peptide Protein Res.*, 1990, **36**, 392; D. F. Mierke, C. Pattaroni, N. Delaet, A. Toy and M. Goodman, *Int. J. Peptide Protein Res.*, 1990, **36**, 418; A. G. Michel, G. Lajoie and C. A. Hassani, *Int. J. Peptide Protein Res.*, 1990, **36**, 489.
7 J. Zabrocki, G. D. Smith, J. B. Jr. Dunbar, H. Iijima and G. R. Marshall, *J. Am. Chem. Soc.*, 1988, **110**, 5875.
8 N. E. Kohl, E. A. Emini, W. A. Schleif, L. J. Davis, J. C. Heimbach, R. A. F. Dixon, E. M. Scolnick and I. S. Sigal, *Proc. Natl. Acad. Sci. USA*, 1988, **85**, 4686.
9 R. E. TenBrink, *J. Org. Chem.*, 1987, **52**, 418.
10 Y. LePage, P. S. White and E. J. Gabe, NRCCAD, An Enhanced CAD-4 Control Program, Annual Meeting of American Crystallographic Association, Hamilton, Ontario, Canada, 1986.
11 E. J. Gabe, Y. LePage, J. P. Charland and F. L. Lee, NRCVAX, An Interactive Program System for Structure Analysis, *J. Appl. Crystallogr.*, 1989, **22**, 384.
12 A. C. Larson, *Acta Crystallogr.*, 1967, **23**, 664.
13 D. T. Cromer and D. T. Waber, *International Tables for X-ray Crystallography*, eds. J. A. Iber and W. C. Hamilton, Birmingham, Kynoch Press (present distributor Kluwer Academic Publisher, Dordrecht), 1974, vol. IV, pp. 99–101.
14 S. W. Homans, R. A. Dwek, D. L. Fernandes and T. W. Rademacher, *Proc. Natl. Acad. Sci. USA*, 1984, **81**, 6286.
15 S. Macura, Y. Huang, D. Suter and R. R. Ernst, *J. Magn. Reson.*, 1981, **43**, 259.
16 SYBYL Molecular Modeling, Version 5.5, Tripos Associate Inc., February 1992.
17 The definition is in agreement with the IUPAC-IUB Joint Commission on Biochemical Nomenclature, *Biochemistry*, 1970, **9**, 3471.

18 A. Michel, G. Villeneuve and J. DiMaio, *J. Comput. Aid. Mol. Design*, 1991, **5**, 553.
19 M. J. S. Dewar, E. G. Zoebish, E. F. Healy and J. J. P. Stewart, *J. Am. Chem. Soc.*, 1985, **107**, 3902.
20 E. Benedetti, G. Morelli, G. Némethy and H. A. Scheraga, *Int. J. Peptide Protein Res.*, 1983, **22**, 1.
21 E. Benedetti, C. Pedone, C. Toniolo, G. Némethy, M. S. Pottle and H. A. Scheraga, *Int. J. Peptide Protein Res.*, 1980, **16**, 156.
22 C. Toniolo, M. Palumbo and E. Benedetti, *Macromolecules*, 1976, **9**, 420.
23 C. G. Suresh and M. Vijayan, *Int. J. Peptide Protein Res.*, 1983, **22**, 617.
24 M. Branik and H. Kessler, *Chem. Ber.*, 1975, **108**, 2176.
25 K. G. R. Pachler, *Spectrochim. Acta*, 1961, **20**, 581; R. J. Abraham and G. Catti, *J. Chem. Soc. B*, 1969, 961.
26 V. F. Bystrov, V. T. Ivanov, S. L. Portnova, T. A. Balashava and Y. A. Ovchinnikov, *Tetrahedron*, 1973, **29**, 873.
27 H. Kessler, *Angew. Chem., Int. Ed. Engl.*, 1982, **21**, 512.
28 I. L. Karle, *J. Am. Chem. Soc.*, 1978, **100**, 1286.
29 R. E. Wolf, Jr., J. A. R. Hartman, J. M. E. Storey, B. M. Foxman and S. R. Cooper, *J. Am. Chem. Soc.*, 1987, **109**, 4328.
30 G. Zanotti, C. Toniolo, T. J. Owen and A. F. Spatola, *Acta Crystallogr., Sect. C*, 1988, **44**, 1576.

Paper 3/07609A
Received 30*th December* 1993
Accepted 15*th March* 1994